fibers

MDPI

Article

Antimicrobial Electrospun Fibers of Polyester Loaded with Engineered Cyclic Gramicidin Analogues

Silvana Maione [1,2], Luis Javier del Valle [1,2,*], Maria M. Pérez-Madrigal [1,2], Carlos Cativiela [3], Jordi Puiggalí [1,2,*] and Carlos Alemán [1,2,*]

1 Departament d'Enginyeria Química, EEBE, Universitat Politècnica de Catalunya, Edifici I.2, C/Eduard Maristany, 10-14, 08019 Barcelona, Spain; silv.maione@gmail.com (S.M.); mar.perez-madrigal@gmail.com (M.M.P.-M.)

2 Research Center for Multiscale Science and Engineering, Universitat Politècnica de Catalunya, C/Eduard Maristany, 10-14, 08019 Barcelona, Spain

3 Departamento de Química Orgánica, Instituto de Síntesis Química y Catálisis Homogénea-ISQCH, CSIC-Universidad de Zaragoza, C/Pedro Cerbuna, 12, 50009 Zaragoza, Spain; cativiela@unizar.es

* Correspondence: luis.javier.del.valle@upc.edu (L.J.d.V.); jordi.puiggali@upc.edu (J.P.); carlos.aleman@upc.edu (C.A.); Tel.: +34-93-721-9678 (L.J.d.V.); +34-93-401-5649 (J.P.); +34-93-401-883 (C.A.)

Academic Editor: Stephen C. Bondy
Received: 30 June 2017; Accepted: 21 August 2017; Published: 11 September 2017

Abstract: Biodegradable polyester fibers have been loaded with two engineered analogues of gramicidin soviet. In these cyclic peptide derivatives, which were designed in a previous work to stabilize the bioactive conformation while enhancing the antimicrobial activity, the D-Phe was replaced by D-Pro, and the L-Pro was changed by 1-aminocyclopropanecarboxylic acid (Ac_3c) or by an Ac_3c derivative with two vicinal phenyl substituents in a trans relative disposition (*S*,*S*-$c_3$diPhe). The diameter, topography, thermal stability and wettability of the polyester fibers, which have been obtained by electrospinning, strongly depend on the molecular constraints and stability of the loaded peptides. More specifically, unloaded and linear gramicidin-loaded fibers (used as control) are hydrophobic, rough and micrometric, while fibers loaded with the cyclic peptides are hydrophilic, ultra-smooth, nanometric and less thermally stable. The activity of the two cyclic peptides increases when loaded into polyester fibers, suggesting that the polymeric matrix stabilizes the bioactive β-sheet structure. The peptide with *S*,*S*-$c_3$diPhe displays higher antibiotic potency and biocompatibility than that with Ac_3c, which indicates not only that the bioactive conformation is better preserved by the former but also the significant role played by the phenyl rings in the recognition by living cells.

Keywords: biocompatibility; conformational restrictions; encapsulation; electrospinning; engineered peptides; hydrophobic peptides

1. Introduction

On-demand release of drug molecules from biomedical devices enables precise targeted dosing that can be temporally tuned to meet the requirements of a variety of biomedical applications [1–3]. Although recent advances have facilitated the use of different stimuli, such as light, magnetic and electric fields, ultrasounds and electrochemical signals, to trigger drug release from smart material formulations (e.g., films, micro- and nanoparticles, and implant devices) [3–6], traditional systems based on the biodegradability of polymeric vehicles remain the most employed technology because of its efficiency, simplicity, and low cost [7–14]. Biodegradable polyester particles and fibers are widely employed for controlled and sustained targeted release of hydrophobic and poorly-water soluble drugs [15–21].

Among biomolecules with therapeutic applications, gramicidin (GA) deserves special mention because of its versatility. From a functional point of view, GA is well known because of its activity as bactericide [22,23], antibiotic [24], and potential therapeutic agent for different carcinomas [25–28]. In spite of its potential biomedical applications, encapsulation of GA has been scarcely studied due to the insolubility of this peptide, which represents a major limitation [19,29–31]. Abdelhamid et al. [29] loaded GA on the surface of graphene oxide (GO) for effective antibacterial treatments. Nevertheless, the utilization of GO for biomedical applications is controversial because of its dose-dependent toxicity to cells and living systems [32]. In addition, peptide particles have been prepared using amino acid sequences related to those of GA [30,31]. Recently, we loaded hydrophobic GA produced by *Bacillus brevis* (i.e., a linear pentadecapeptide with sequence formyl-L-Xxx-Gly-L-Ala-D-Leu-L-Ala-D-Val-L-Val-D-Val-L-Trp-D-Leu-L-Yyy-D-Leu-L-Trp-D-Leu-L-Trp-ethanolamine, where Xxx can be either Val or Ile and Yyy is frequently Trp) into spherical microparticles (average diameter: 5.0 μm ± 0.7 μm) of poly(tetramethylene succinate) (PE44), a biodegradable and biocompatible aliphatic polyester, by means of electrospraying [19]. Unfortunately, the release of GA in physiological media was severely limited by the very low solubility of the biomolecule in aqueous solution: a fast burst effect followed by the establishment of equilibrium after five days was observed in hydrophilic media. However, despite such limitation, biological tests demonstrated that GA retained its antimicrobial activity after loading and did not alter the biocompatibility of PE44 [19].

The high potential of peptides in diagnosis and therapeutics is sometimes hampered by their short-life times (i.e., endogenous proteases rapidly digest these biomolecules). Among the different strategies proposed to protect peptides from proteolytic cleavage, targeted replacements with non-coded amino acids are among the most successful ones [33–35]. In an early study, Cativiela and co-workers designed and synthetized two rigid GA analogues by introducing some chemical changes at the sequence of gramicidin soviet (GA-S) to enhance the antimicrobial activity of GA by stabilizing the bioactive conformations through steric and stereochemical constraints [36]. In addition, the incorporation of non-proteinogenic residues into GA-S should also impart stability against proteolytic cleavage. GA-S is a cyclic symmetrical cationic antimicrobial peptide of sequence cyclo(Val-Orn-Leu-D-Phe-Pro)$_2$ produced non-ribosomally by *Bacillus brevis* [37] and active against bacteria and fungi [38,39]. More specifically, in such two engineered peptides, the D-Phe was replaced by D-Pro while the L-Pro was changed by two conformationally restrained residues. In the first peptide, hereafter denoted GA-S1 (with sequence cyclo(Val-Orn-Leu-D-Pro-Ac$_3$c)$_2$), L-Pro was replaced by 1-aminocyclopropanecarboxylic acid (Ac3c in Scheme 1), an α,α-dialkylated amino acid with strong stereochemical constraints [40,41]. The second peptide (with sequence cyclo(Val-Orn-Leu-D-Pro-*S*,*S*-c$_3$diPhe)$_2$), hereafter denoted GA-S2, was designed using an Ac3c derivative with two vicinal phenyl substituents in a trans relative disposition (*S*,*S*-c$_3$diPhe in Scheme 1) to replace L-Pro. It is worth noting that *S*,*S*-c$_3$diPhe is much more constrained and hydrophobic than Ac$_3$c because of two additional phenyl rings [42]. Moreover, the substitutions introduced in GA-S1 and GA-S2 are expected to have a severe impact on the capacity of the peptides to be loaded in polymeric matrices since they reduced the molecular flexibility and altered the wettability.

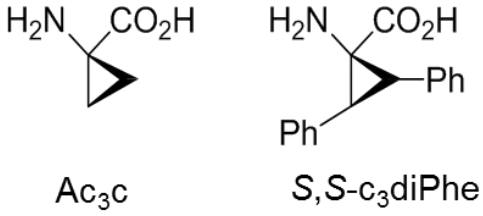

Scheme 1. Chemical structure of Ac$_3$c and *S*,*S*-c$_3$diPhe.

In this work, we prepared ultrathin fibers loaded with GA-S1 and GA-S2 using electrospinning. This electrostatic technique involves the use of a high voltage field to charge the surface of a polymer

solution droplet, which is held at the end of a capillary tube, inducing the ejection of a liquid jet towards a grounded target (collector) [43–45]. After characterizing the morphology, chemical structure, and properties of the resulting GA-loaded PE44 fibers, we examined their antibiotic potency and biocompatibility as well as the peptide release in different environments. In all cases, results were compared with those obtained from PE44 fibers loaded with linear GA pentadecapeptide, hereafter denoted GA-L. PE44 fibers stabilize the bioactive conformation of the two cyclic peptides and regulate the peptide release in hydrophilic environments, which is of crucial importance for biomedical applications. Furthermore, PE44/GA-S2 is more effective than PE44/GA-S1 in terms of antimicrobial response because of the disposition of the phenyl rings in *S*,*S*-$c_3$diPhe.

2. Materials and Methods

2.1. Materials

PE44 is a commercial product (Bionolle® 1001) supplied by Showa Denko K.K. (München, Germany). The polymer has a melt flow index of 1.6 g/10 min (measured at 190 °C under a load of 2.16 kg according to ASTM-D1238). Linear GA was purchased from Sigma-Aldrich (G5002, St. Luis, MO, USA), while GA-S1 and GA-S2 were prepared as previously reported [36].

2.2. Electrospinning

Mixtures of PE44 and GA peptides (i.e., GA-S1, GA-S2 and GA-L) were electrospun, samples being named PE44/GA-# (where GA-# indicates the loaded peptide). Mixtures were prepared as follows. PE44 was dissolved in chloroform while peptides were dissolved in ethanol. Solutions were kept under stirring at 80 rpm overnight. Finally, the solutions were mixed and loaded in a 5 mL BD (Becton Dickson Co., Franklin Lakes, NJ, Spain) plastic syringe for delivery through an 18 G × 1.1/2″ needle at a mass-flow rate of 2 mL/h using a KDS100 infusion pump. The PE44 concentration was 13.0 wt % in the electrospinning mixtures with GA-L and 2 wt % in mixtures with GA-S1 and GA-S2. The concentrations of peptides were 1.3 wt % for GA-L and 0.2 wt % for both GA-S1 and GA-S2. As a control, fibers of pure PE44 were produced using a 13 w/v % concentration of polymer. The applied voltage was 15 kV for PE44/GA-S1 and PE44/GA-S2, while for unloaded PE44 (control) and PE44/GA-L fibers, the applied voltage was 25 kV. All electrospun nanofibers were obtained using a needle tip-collector distance of 18 cm. The choice of these conditions should be mentioned (i.e., concentrations, distance between the syringe tip and the collector, voltage and the flow rate) were selected on the basis of preliminary experiments devoted to optimize the morphology of the fibers. Thus, appropriate selection of the processing conditions is required to avoid the formation of droplets and electrospun beads. The procedure used for such optimization, which was individually applied for each mixture, was detailed in previous works [20,21].

2.3. Circular Dichroism (CD)

CD measurements were carried out in a Jasco J-810 spectropolarimeter (Jasco Inc., Easton, MD, USA) at 22 °C using a quartz cuvette. The CD data were recorded with standard sensitivity (100 mdeg), in the 190–350 nm range, with bandwidth of 2 mm, response time of 0.5 s and scanning speed of 500 nm/min. The reported spectra correspond to the average of five scans, the raw spectra being smoothed by the Savitsky–Golay algorithm. Spectra were analyzed in the DicroWeb software (version 1.0, Birkbeck College, University of London, London, UK) [46–48].

2.4. Microscopy

Optical microscopy (OM) studies were performed with a Zeiss Axioskop 40 microscope. Micrographs were taken with a Zeiss AxiosCam MRC5 digital camera (Carl Zeiss, Göttingen, Germany).

Detailed inspection of texture and morphology of microspheres was conducted by scanning electron microscopy (SEM) using a Focus Ion Beam Zeiss Neon 40 instrument (Zeiss, Oberkochen,

Germany). Carbon coating was accomplished using a Mitec K950 Sputter Coater (Quorum Technologies Ltd., Ashford, UK) fitted with a film thickness monitor *k*150×. Samples were visualized at an accelerating voltage of 5 kV. The diameter of the nanofibers was measured with the SmartTiff software (Version 1.0) from Carl Zeiss SMT Ltd (Göttingen, Germany).

Atomic Force Microscopy (AFM) was conducted to obtain topographic and phase images of the surface of fibers using silicon TAP 150-G probes (Budget Sensors, Sofia, Bulgaria) with a frequency of 150 kHz and a force constant of 5 N/m. Images were obtained with an AFM Dimension microscope using the NanoScope IV controller (Veeco Instruments Inc., New York, NY, USA) under ambient conditions in tapping mode. The row scanning frequency was set between 0.4 and 0.6 Hz. The Root Mean Square roughness (RMS R_q), which is the average height deviation taken from the mean data plane, was determined using the statistical application of the NanoScope Analysis software (1.20, Veeco Instruments Inc., New York, NY, USA).

2.5. Chemical Characterization

Infrared spectroscopy was used to assess the presence of peptide in PE44/GA-S1, PE44/GA-S2 and PE44/GA-L samples. Absorption spectra were recorded with a Fourier Transform FTIR 4100 Jasco spectrometer (Jasco International Co. Ltd., Tokyo, Japan) in the 4000 cm^{-1}–600 cm^{-1} range. A Specac model MKII Golden Gate (Specac Ltd., Orpington, UK) attenuated total reflection (ATR) with a heated Diamond ATR Top-Plate was used.

X-Ray photoelectron spectroscopy (XPS) analyses were performed in a SPECS system (Berlin, Germany) equipped with a high-intensity twin-anode X-ray source XR50 of Mg/Al (1253 eV/1487 eV) operating at 150 W, placed perpendicular to the analyzer axis, and using a Phoibos 150 MCD-9 XP detector (SPECS system, Berlin, Germany). The X-ray spot size was 650 mm. The pass energy was set to 25 eV and 0.1 eV for the survey and the narrow scans, respectively. Charge compensation was achieved with a combination of electron and argon ion flood guns. The energy and emission currents of the electrons were 4 eV and 0.35 mA, respectively. For the argon gun, the energy and the emission currents were 0 eV and 0.1 mA, respectively. The spectra were recorded with a pass energy of 25 eV in 0.1 eV steps at a pressure below 6×10^{-9} mbar. These standard conditions of charge compensation resulted in a negative but perfectly uniform static charge. The C 1s peak was used as an internal reference with a binding energy of 284.8 eV. High-resolution XPS spectra were acquired by Gaussian/Lorentzian curve fitting after S-shape background subtraction. The surface composition was determined using the manufacturer's sensitivity factors.

2.6. Properties

Thermal degradation was studied at a heating rate of 20 °C/min (sample weight ca. 5 mg) with a Q50 thermogravimetric analyzer of TA Instruments (TA instruments, New Castle, DE, USA) and under a flow of dry nitrogen. Test temperatures ranged from 30 °C to 600 °C.

Contact angle measurements were carried out using the water sessile drop method. Images of milliQ water drops (0.5 μL) were recorded after stabilization with the equipment OCA 15EC (Data-Physics Instruments GmbH, Filderstadt, Germany). SCA20 software (Version 2.0, Data-Physics Instruments GmbH, Filderstadt, Germany) was used to analyze the images and determine the contact angle value, which was obtained as the average of at least six independent measures for each sample.

2.7. Release Experiments

Mats with peptide-loaded fibers were cut into 2×2 cm^2 squares (around 15 mg–20 mg of weight), which were weighed and placed into polypropylene tubes. Phosphate buffer saline (PBS, pH 7.4) and PBS supplemented with 70 *v*/*v*-% of ethanol (PBS-EtOH) were considered as release media. The addition of ethanol to hydrophilic PBS increases the hydrophobicity of the medium and provokes some swelling effect, both favoring the release of hydrophobic drugs. The released peptide was quantified using the Bradford reagent. Assays were carried out by immersing sample mats in 30 mL

of the release medium at 37 °C for 1 week. Aliquots (1 mL) were drawn from the release medium at predetermined time intervals, and an equal volume of fresh medium was added to the release vessel. The Bradford reaction was performed in microtiter plate mode and the absorbance measurement in a reader plate. Calibration curves were obtained by plotting the absorbance measured at 595 nm against drug concentration. Finally, the mats were dissolved in chloroform and the residual drug was extracted in ethanol for quantification. All tests were performed in triplicate to control the homogeneity of the release, and the results were averaged.

2.8. Inhibition of Bacterial Growth

Escherichia coli (*E. coli*), *Proteus vulgaris* (*P. vulgaris*), *Citrobacter freundii* (*C. freundii*), *Klebsiella pneumoniae* (*K. pneumoniae*), *Staphylococcus aureus* (*S. aureus*), *Staphylococcsu epidemidis* (*S. epidermidis*), *Bacillus cereus* (*B. cereus*) and *Micrococcus luteus* (*M. luteus*) were selected to evaluate the antibacterial activity of peptides loaded in fibers. The bacteria were previously grown aerobically to exponential phase in lysogeny broth (LB) (Lennox) (tryptone 10 g; yeast extract 5 g, NaCl 5 g, pH 7.2).

Growth experiments were performed placing five pieces (area: 0.5 cm^2) of each sample in tubes of 15 mL. After this, 2 mL of broth culture containing 1×10^3 colony forming units (CFU) was seeded in each samples-containing tube. The cultures were incubated at 37 °C and agitated at 100 rpm. Aliquots of 100 μL were taken at predefined time intervals for absorbance measurement at 650 nm in a plate reader. Thus, turbidity was directly related to bacterial growth. The bacterial growth in broth culture alone (in absence of any material) was considered as the maximum growth (control) and it was used to calculate the relative growth of the bacteria in presence of the samples. Values were averaged considering the five replicas.

Agar diffusion tests were performed in Petri dishes of 90 mm, and seeded separately with 1.5×10^8 CFU/mL of each bacterium. Disks of 0.5 cm of diameter for each sample were placed onto an agar diffusion plate. In addition to PE44/GA-S1, PE44/GA-S2 and PE44/GA-L samples, assays were carried out using discs of gentamicin (GM), an antibiotic used to treat many types of bacterial infections, as positive control. Inhibition halo images were taken after incubation of samples with bacteria for 24 h at 37 °C.

2.9. Cytotoxicity and Cell Adhesion

Madin Darby canine kidney (MDCK) cells were cultured in Dulbecco Modified Eagle Medium (DMEM) high glucose supplemented with 10 % *v*/*v* fetal bovine serum (FBS), penicillin (100 units/mL), and streptomycin (100 μg/mL). Cultures were maintained in a humidified incubator with an atmosphere of 5% CO_2 and 95% O_2 at 37 °C. Culture media were changed every two days. When the cells reached 80%–90% confluence, they were detached using 1 mL–2 mL of trypsin (0.25% trypsin/EDTA) for 5 min at 37 °C. Finally, cells were re-suspended in 5 mL of fresh medium, their concentration being determined by counting in a Neubauer camera (Optisum, New York, NY, USA) using 0.4% trypan blue as a dye vital.

Unloaded PE44, PE44/GA-S1, PE44/GA-S2 and PE44/GA-L samples were placed in plates of 24 wells and sterilized using UV-light for 15 min in a laminar flux cabinet. Controls were simultaneously performed by culturing cells on the surface of the tissue culture polystyrene (TCPS) plates. For adhesion assays, an aliquot of 50 μL containing 5×10^4 cells was deposited onto each sample. Then, cell attachment was promoted by incubating under culture conditions for 30 min. Finally, 500 μL of the culture medium were added to each well. After 24 h, non-attached cells were washed out, while attached cells were quantified. Cytotoxicity was also determined after 24 h of culture. All viability measures were relative to TCPS used as control (i.e., 100%).

Viability for cytotoxicity and cellular adhesion were evaluated by the colorimetric 3-(4,5-dimethylthiazol-2-yl)-2,5-diphenyltetrazolium bromide (MTT) assay. This assay measures the ability of the mitochondrial dehydrogenase enzyme of viable cells to cleave the tetrazolium rings of the MTT and form formazan crystals, which are impermeable to cell membranes and, therefore, are accumulated

in healthy cells. This process is detected by a color change: the characteristic pale yellow of MTT transforms into the dark-blue of formazan crystals. Specifically, 50 µL of MTT solution (5 mg/mL in PBS) were added to each well. After 3 h of incubation, samples were washed twice with PBS and placed in clean wells. In order to dissolve formazan crystals, 200 µL of DMSO/methanol/water (70/20/10% *v*/*v*) was added. Finally, the absorbance at 570 nm was measured using a microplate reader (Biochrom EZ Rea 400d, Harvard Bioscience, Harvard, NE, USA). The resulting viability results were normalized to TCPS control as relative percentages. Results were derived from the average of six replicates ($n = 6$) for each independent experiment. ANOVA and Tukey tests were performed to determine statistical significance, which was considered at a confidence level of 95% ($p < 0.05$).

3. Results

3.1. Electrospinning of PE44 and Peptide Mixtures

Firstly, we aimed to load GA-S1 and GA-S2 in electrosprayed PE44 microspheres, as we successfully did for GA-L [19]. However, despite the high peptide-loading efficiency (41%) and well-defined morphology of PE44/GA-L microspheres (Figure 1a), PE44/GA-S1 and PE44-GA-S2 microspheres were not feasible, even after optimization of the processing conditions. This important drawback, which was mainly attributed to the conformational rigidity of the two modified cyclic peptides, led us to consider the use of electrospun fibers as the most suitable system for the loading and sustained delivery of GA-S1 and GA-S2.

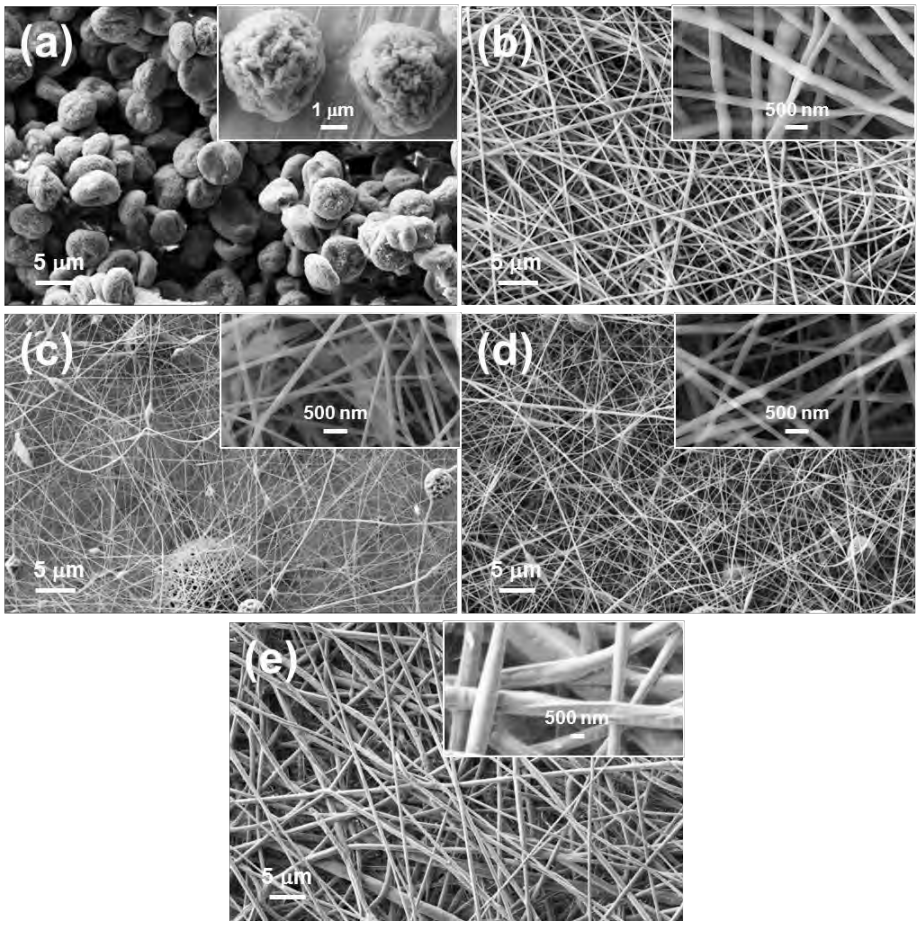

Figure 1. High and low magnification SEM micrographs of (**a**) PE44/GA-L electrosprayed microspheres (experimental conditions defined in reference 19); (**b**) unloaded PE44; (**c**) PE44/GA-S1; (**d**) PE44/GA-S2 and (**e**) PE44/GA-L electrospun fibers.

PE44 and GA peptides (i.e., GA-S1, GA-S2, and GA-L) were dissolved in chloroform and ethanol, respectively, for the electrospinning process. Accordingly, in a first stage, we examined the stability of the three peptides in both solvents using circular dichroism (CD) spectroscopy, and the recorded spectra were interpreted using the on-line Dichroweb software [46–48]. In ethanol, the three peptides exhibit secondary structures (Figure 2a). More specifically, the spectrum of GA-S2 was interpreted as a combination of β-sheet (83%), β-turn (9%), and disordered (8%) motives, which was fully consistent with the reported 2D NOESY spectra recorded in H_2O/D_2O 9:1 v/v [36]. In contrast, GA-S1 and GA-L exhibited a combination of regular and distorted α-helical structures with a small fraction of disordered motives (< 5%). It is worth noting that the antibiotic activity of GA-S and GA-L is associated with β-sheet and α-helical conformation, respectively [24,38,39]. Therefore, the antimicrobial potency of GA-S2 and GA-L is expected to be preserved in ethanol, while that of GA-S1 could be affected by peptide–solvent interactions. In the following sections, we demonstrate that the antibiotic potency is higher for GA-S2 than for GA-S1, even though the microbicide activity of the latter is not negligible. Unfortunately, the complexity of the CD spectra recorded in chloroform (Figure 2b) precluded their analysis, thus suggesting a complex mixture of ordered structures [49].

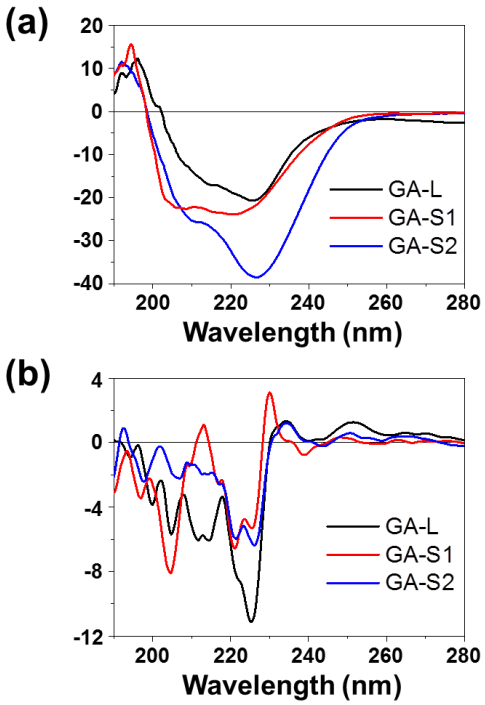

Figure 2. Circular dichroism spectra of GA-S1, GA-S2 and GA-L recorded in (**a**) ethanol and (**b**) chloroform. The peptide concentration was 5 mg/mL in all cases.

Mixtures of PE44 and GA peptides (i.e., GA-S1, GA-S2 and GA-L) were electrospun to obtain PE44/GA-# fibers, where GA-# indicates the loaded peptide. For each case, the processing conditions (i.e., concentrations, distance between the syringe tip and the collector, voltage, and flow rate) were optimized to avoid the formation of droplets and electrospun beads. The feeding mixture essentially depended on the peptide to be accommodation within the polymeric matrix, which is conditioned by the peptide conformational flexibility. After optimization, the PE44 concentration in the electrospinning mixtures was 13.0 wt % for unloaded and GA-L loaded fibers, while it decreased to 2 wt % for GA-S1 and GA-S2 loaded fibers. The concentrations of peptides were 1.3 wt % for GA-L and 0.2 wt % for both GA-S1 and GA-S2. It is worth noting that the amount of peptide used in the feeding solution is completely incorporated into the fibers.

Figures 3 and 1b–e compare representative optical microscopy (OM) and scanning electron microscopy (SEM) micrographs, respectively, of unloaded PE44, PE44/GA-S1, PE44/GA-S2 and PE44/GA-L, while their average diameters (*D*) are listed in Table 1. Although both unloaded PE44 and PE44/GA-L resulted in well-defined fibers, the loading of GA-L caused some important changes. Specifically, unloaded PE44 fibers presented a cylindrical morphology with D = 246 nm ± 68 nm, while the linear peptide induced a flatter morphology (ribbon-like fibers) and a significant increment in the fiber thickness (D = 590 nm ± 156 nm). In contrast, PE44/GA-S1 and PE44/GA-S2 fibrous mats displayed a high amount of droplets and beads, even after optimization of the processing conditions. Furthermore, the cylindrical fibers experienced a drastic reduction in diameter (D = 106 nm ± 25 nm and 146 nm ± 34 nm for PE44/GA-S1 and PE44/GA-S2, respectively). These phenomena have been attributed to the low polymer concentration in the feeding solution, which could not be increased in order to keep a reasonable viscosity of this solution and a high drug/polymer ratio.

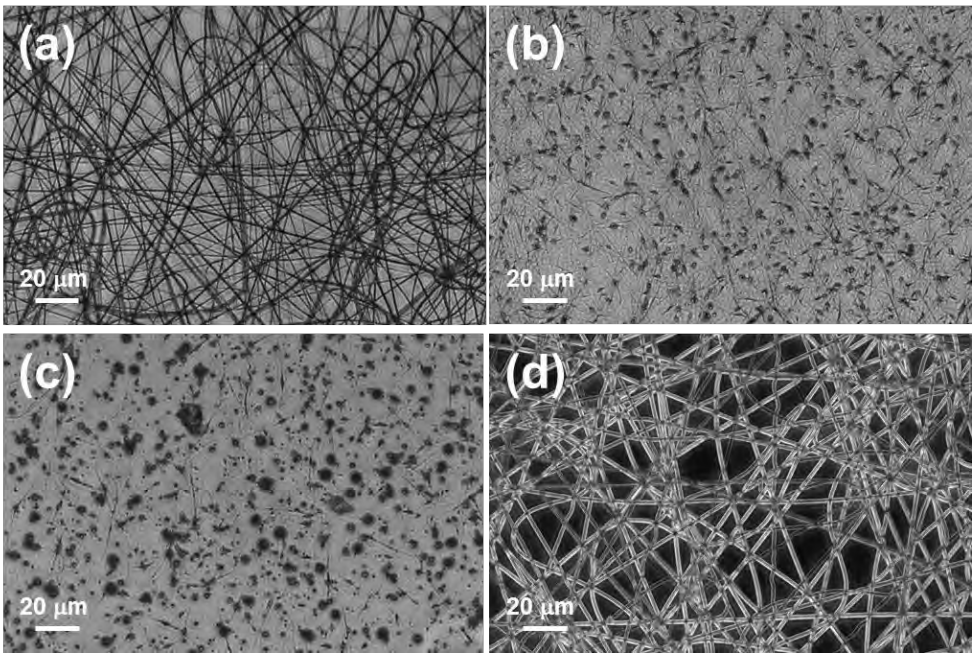

Figure 3. Optical microscopy micrographs of (**a**) unloaded PE44, (**b**) PE44/GA-S1, (**c**) PE44/GA-S2 and (**d**) PE44/GA-L electrospun nanofibers.

Table 1. Average diameter (*D*), root-mean-square roughness (RMS R_q), temperatures for 50% and 70% weight loss ($T_{50\%}$ and $T_{70\%}$, respectively), maximum temperature (T_{max}) and contact angle (θ).

	***D* (nm)**	**RMS R_q (nm)**	**$T_{50\%}$ (°C)**	**$T_{70\%}$ (°C)**	**T_{max} (°C)**	**θ (°)**
Unloaded PE44	246 ± 68	36.2 ± 8.7	410	420	419	125 ± 6
PE44/GA-S1	106 ± 25	6.1 ± 2.4	400	410	412	128 ± 4
PE44/GA-S2	146 ± 34	5.0 ± 1.7	387	400	401	47 ± 1
PE44/GA-L	590 ± 156	36.8 ± 3.6	405	416	415	68 ± 2

3D topographic atomic force microscopy (AFM) images, which are displayed in Figure 4, are in good agreement with SEM observations. In addition, comparison between the topographic and phase AFM images indicates that the peptides are not located as particles or aggregates on the surface of the fibers. In addition, the root-mean-square roughness (RMS R_q) values, which are included in Table 1, evidenced that PE44/GA-S1 and PE44/GA-S2 nanofibers are ultra-smooth, while the texture of PE44 fibers is not altered by GA-L.

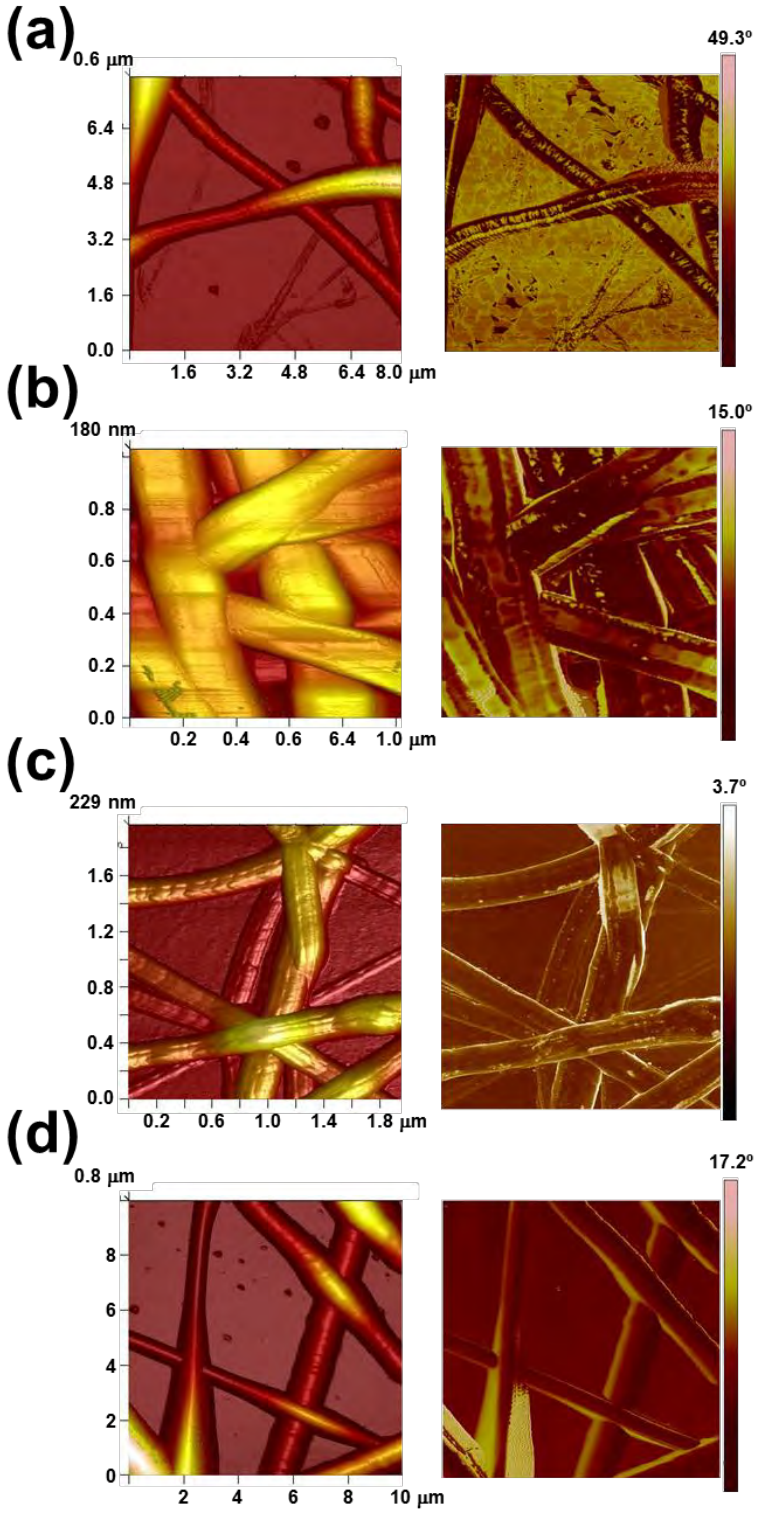

Figure 4. AFM images of (**a**) unloaded PE44, (**b**) PE44/GA-S1, (**c**) PE44/GA-S2 and (**d**) PE44/GA-L electrospun fibers: 3D topography (left) and phase (right) images. The scan window size was adjusted in each case according to the diameter of the fibers (see Table 1): (**a**) 8 × 8 µm^2; (**b**) 1 × 1 µm^2; (**c**) 2 × 2 µm^2; and (**d**) 10 × 10 µm^2.

3.2. Chemical Characterization

Figure 5a displays the FTIR spectra of unloaded PE44, PE44/GA-S1, PE44/GA-S2 and PE44/GA-L samples. In the spectrum of PE44, the peaks corresponding to the C=O and C–O–C vibrations of the ester bond are detected at 1712, 1150 (sharp and strong absorption bands) and 1044 cm^{-1} (sharp and medium absorption band). These important bands are also clearly identified in the spectra of the three peptide-loaded PE44 samples (red rectangles in Figure 5a). Other main absorption bands of PE44 appearing at 2964, 2946 and 2857 cm^{-1} are attributed to the C–H aliphatic stretching; CH_2 asymmetric and symmetric bending are shown between 1470 cm^{-1} and 1390 cm^{-1}; $–(CH_2)_n–$ hydrocarbon chains are detected at 804 cm^{-1} (sharp) and 748 cm^{-1} (broad, CH_2 rock vibrations).

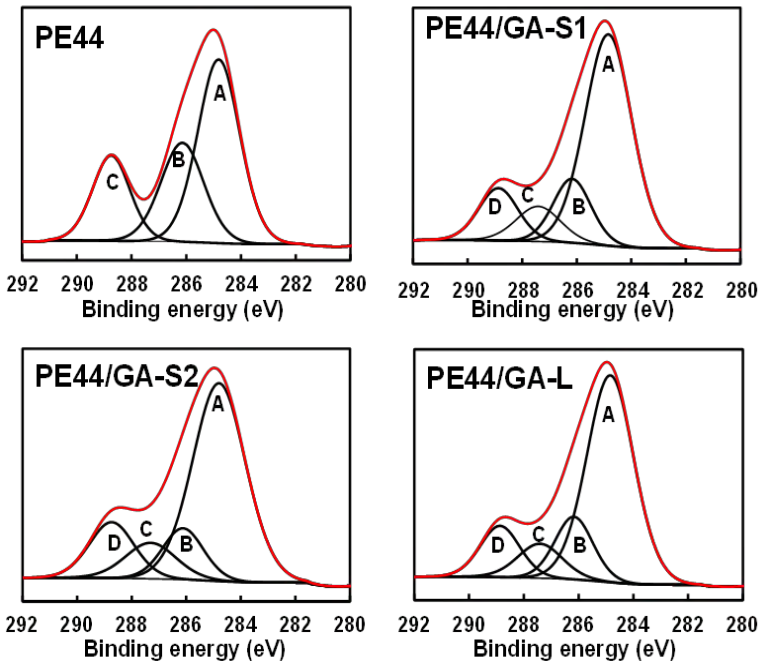

Figure 5. High-resolution XPS spectrum at the C 1s region for unloaded and GA-loaded PE44 fibers. The red line corresponds to the experimental profile while the black lines are the peaks from deconvolution. Unloaded PE44: C–C/C–H (A: 284.8 eV), C–O (B: 286.1 eV) and C=O (C: 288.7 eV). GA-S1, GA-S2 and GA-L loaded PE44: C–C/C–H (A: 284.9 eV), C–O (B: 286.2 eV), (O=)C–NH peptide bond (287.7) and C=O (C: 288.8 eV).

Most importantly, the successful loading of the peptide in PE44/GA-S1, PE44/GA-S2 and PE44/GA-L samples is evidenced in Figure S1 by the bands arising from the amide groups. The amide II band, which is due to the C–N stretching vibration in combination with N–H bending, is detected at ~1540 cm^{-1} (i.e., 1539 cm^{-1}, 1537 cm^{-1} and 1541 cm^{-1} for PE44/GA-S1, PE44/GA-S2, and PE44/GA-L, respectively). The amide I band, which arises from the C=O stretching vibration of the peptide bond and is modulated by the peptide secondary structure, appears at 1629 cm^{-1} for the systems loaded with cyclic peptides and at 1635 cm^{-1} for PE44/GA-L. The C=O stretching of aliphatic esters, which corresponds to the intense and sharp band at 1712 cm^{-1} for unloaded and peptide-loaded PE44 samples, is clearly distinguishable from such two amide bands.

The chemical structure of the systems under study was further characterized by X-ray photoelectron spectroscopy (XPS). Table 2 compares the atomic composition of unloaded and peptide-loaded PE44 fibers. The detection of a small percentage of nitrogen in unloaded PE44 samples has been attributed to the substrate (aluminum foil) used to collect the fibers during electrospinning. However, the percentage of nitrogen increases from 0.26% in unloaded PE44 to 5.58%, 3.11%, and 6.52% in PE44/GA-S1, PE44/GA-S2, and PE44/GA-L, respectively, which further confirms the successful incorporation

of the peptides. High-resolution XPS spectra in the C 1s region are displayed in Figure 5, while those in the N 1s and O 1s regions are displayed in Figure 6. The three Gaussian curves derived from the deconvolution of the C 1s peak for unloaded polyester fibers correspond to the saturated C–C/C–H (284.8 eV), C–O (286.1 eV) and C=O (288.7 eV) bonds of the PE44 chains [50,51]. The three peptide-loaded PE44 fibers display an additional fourth Gaussian curve at 287.7 eV that has been attributed to the (O=)C–NH peptide bonds [52,53]. On the other hand, two Gaussian curves, which correspond to the C=O (531.87 eV) and C–O bonds (533.42), were derived from the O 1s signal [50–54]. The intensity of the C=O component is lower than that of the C–O one for unloaded PE44, while the opposite is obtained for PE44/GA-S1, PE44/GA-S2, and PE44/GA-L due to the incorporation of peptides.

Table 2. Atomic percent composition (C 1s, N 1s and O 1s) obtained by XPS for unloaded PE44, PE44/GA-S1, PE44/GA-S2 and PE44/GA-L.

	C 1s (%)	N 1s (%)	O 1s (%)
Unloaded PE44	69.23	0.26	30.51
PE44/GA-S1	67.77	5.58	26.65
PE44/GA-S2	66.63	3.11	30.26
PE44/GA-L	70.13	6.52	23.25

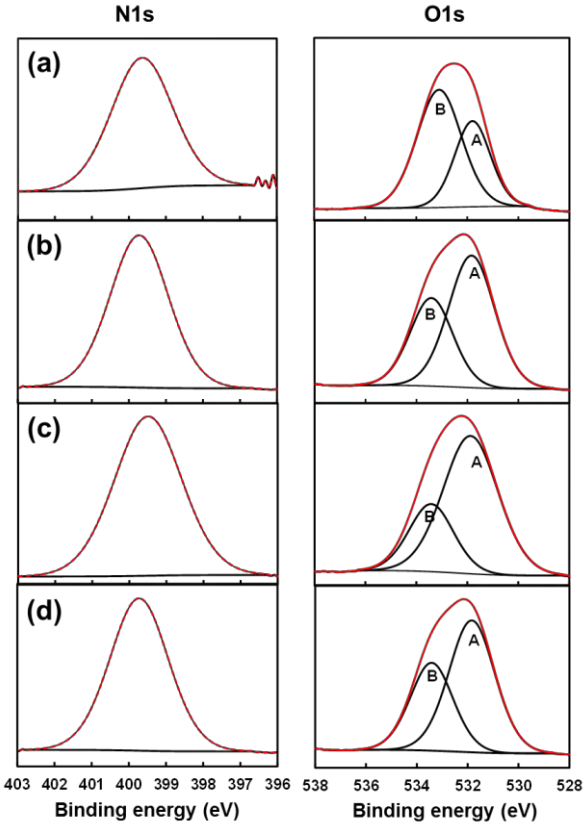

Figure 6. High-resolution XPS spectra for (**a**) unloaded PE44; (**b**) PE44/GA-S1; (**c**) PE44/GA-S2 and (**d**) PE44/GA-L: N 1s and O 1s regions. The red line corresponds to the experimental profile while the black lines are the peaks from deconvolution.

3.3. Properties

Thermogravimetric analyses (Figure 7a and Table 1) reflect the significant influence of the peptide in the thermal stability of PE44. Although all loaded samples are stable up to a temperature 40 °C

higher than the melting temperature of the PE44 matrix (T_m = 112.8 °C) at least, the thermal stability of PE44/GA-S1 and, especially, PE44/GA-S2 is considerably lower than that displayed by PE44/GA-L and unloaded PE44, which are very similar. Thus, the temperatures at a 50% weight loss ($T_{50\%}$) are around 10 °C and 23 °C lower for PE44/GA-S1 and PE44/GA-S2, respectively, than for unloaded PE44. Moreover, these differences are preserved at a 70% weight loss ($T_{70\%}$, Table 1). Differential thermogravimetric analysis (DTGA) curves show a pronounced degradation step for all peptide-loaded samples, the maximum temperature (T_{max}, Table 1) increasing as follows: GA-S2 < GA-S1 < GA-L. Furthermore, an initial degradation step at 224 °C and 241 °C occurs for PE44/GA-S1 and PE44/GA-S2, respectively, which involved a weight loss lower that 5%. This degradation is probably induced by the severe molecular constraints of Ac_3c and *S*,*S*-$c_3$diPhe in the cyclic peptides, thus being less stable than GA-L. No significant char (i.e., less than 2.5%) was observed at temperatures higher than 500 °C. Therefore, the peptide clearly influences the thermal stability of the polymeric matrix, which is practically independent of the morphology. For instance, the thermal parameters for unloaded PE44 and PE44/GA-L microspheres (average particle diameter: 5.1 μm ± 0.5 μm and 5.0 μm ± 0.7 μm, respectively), $T_{50\%}$ = 410 °C and 405 °C, $T_{70\%}$ = 420 °C and 416 °C, and T_{max} = 418 °C and 411 °C [19], are similar to those listed in Table 1 for fibers.

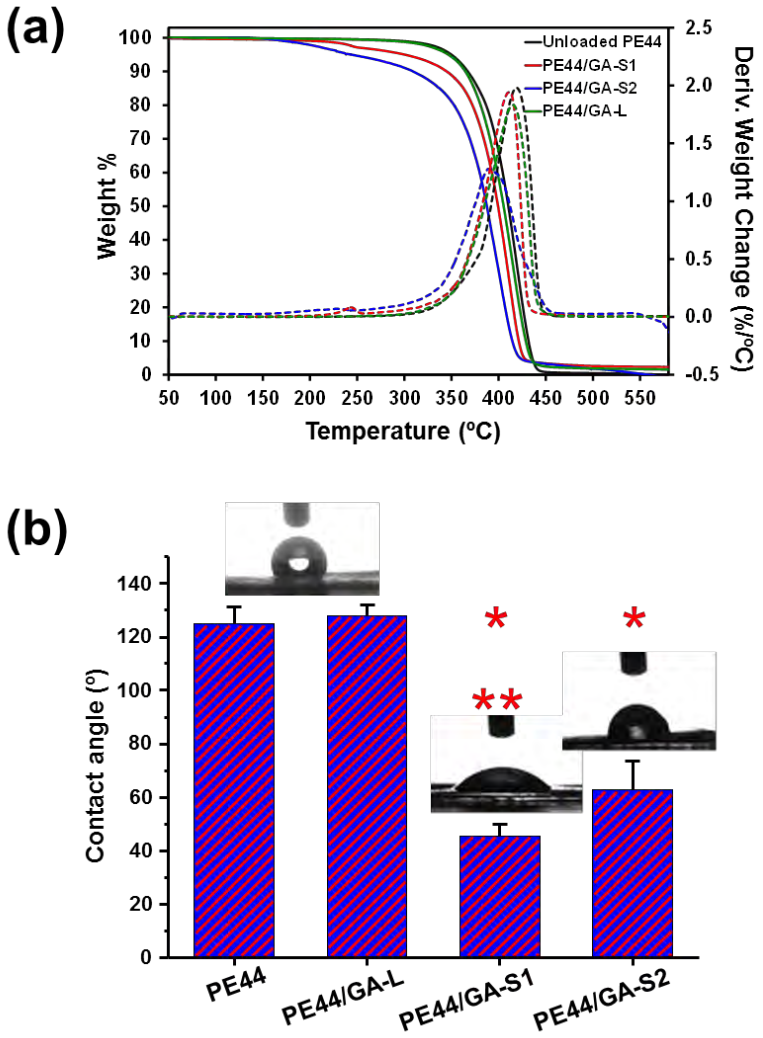

Figure 7. For unloaded PE44, PE44/GA-S1, PE44/GA-S2 and PE44/GA-L electrospun fibers: (**a**) TGA (solid lines) and DTGA (dashed lines) curves; and (**b**) contact angle. * Significantly different with respect to unloaded PE44 and PE44/GA-L with $p < 0.05$. ** Significantly different with respect to PE44/GA-S2 with $p < 0.05$.

The contact angle values (θ) measured using water (Figure 7b) indicate that unloaded PE44 matrices are hydrophobic (θ = 125° ± 6°) due to both the presence of aliphatic segments and the microfibrous structure of produced electrospun mats. In contrast, the water contact angle value determined for unloaded PE44 electrosprayed microspheres was significantly lower (θ = 104° ± 3°) [19], even though the surface RMS Rq was slightly higher for microspheres than for fibers. This feature proves that the wettability of structured polymeric matrices is influenced by morphology. Such hydrophobic character is retained after loading GA-L (i.e., θ = 128° ± 4° for PE44/GA-L), whereas the presence of GA-S1 and GA-S2 transformed the PE44 fiber mats into hydrophilic substrates (θ = 47° ± 1° and 68° ± 2° for PE44/GA-S1 and PE44/GA-S2, respectively). The Wenzel equation indicates that, if the surface is chemically hydrophobic, as that of PE44, it will become less hydrophobic when the surface roughness decreases [55]:

$$\cos\theta_m = r \cdot \cos\theta, \quad (1)$$

where θ_m is the measured contact angle, θ_γ is the Young contact angle and r is the roughness ratio, the latter parameter increasing with the RMS R_q (Table 1). The Wenzel equation is based on the assumption that the liquid penetrates into the rough grooves, which occurs when the droplet is larger than the roughness scale by two or three orders of magnitude, as it is in this case. However, other factors are probably affecting the wettability of PE44/GA-S1 and PE44/GA-S2, since the reduction of the contact angle with respect to unloaded PE44 and PE44/GA-L is too high to be attributed exclusively to the surface roughness. Thus, the distribution of GA-S1 and GA-S2 peptides in the polymeric matrix is possibly another factor influencing the wettability of the PE44 fibers. More specifically, a homogeneous distribution of the cyclic peptides on the surface of fibers, forming aggregates small enough to be undetectable by phase imaging AFM, would result in a reduction of the contact angle due to the exposition of amide groups. This situation is completely different from that of hydrophobic PE44/GA-L fibers, for which their resemblance with unloaded PE44 fibers suggests that the peptide is inside the polymeric matrix.

3.4. Peptide Release

The peptide release profiles in PBS, which is the simplest physiological medium, for GA-S1, GA-S2 and GA-L loaded fibers are displayed in Figure 8a. The cumulative release plots in PBS indicate a massive initial burst release up to a maximum percentage (65 ± 3%, 78 ± 1% and 74 ± 3% for GA-S1, GA-S2 and GA-L, respectively) and a subsequent decrease of the release percentage until a value of ~40–50%, depending on the peptide. This behavior suggests that, after an initial burst release caused by the rapid diffusion of PBS into PE44 fibers, a given amount of such delivered peptide re-enters in the PE44 fibers to meet equilibrium conditions. These observations, especially for PE44/GA-S1 and PE44/GA-S2, are consistent with the location of the peptide near the surface, as suggested by contact angle measurements. After the initial burst release, the shape of the cumulative profiles is similar regardless the loaded peptide, even though the release rate to the medium highly depends on the chemical structure of the peptide. For example, the release after 24 h reaches values of 55 ± 6%, 49 ± 2% and 35 ± 2% for GA-S1, GA-S2 and GA-L, respectively, increasing to 86 ± 1%, 70 ± 4% and 57 ± 2% after 48 h. The complete stabilization of the amount of released peptide, which was reached after ~5 days, occurred at 97 ± 1%, 78 ± 2% and 62 ± 4% for GA-S1, GA-S2 and GA-L, respectively.

After the initial burst, the release kinetics can be explained in all cases by the Higuchi and first-order models. On the one hand, the Higuchi model, which provides a linear behavior when the cumulative percentage of peptide release is represented against the square root of time, indicates that: (i) the concentration of peptide in the matrix is much higher than the peptide solubility; (ii) the peptide aggregates are significantly smaller than the system thickness; (iii) the PE44 swelling and diffusivity are very low; and (iv) the peptide diffusivity is constant. On the other hand, the first order model results in a straight line when the data are plotted as the logarithm of the cumulative percentage of peptide release versus time, which reflects that the PE44 mat can be considered as a porous matrix.

It is worth highlighting that the Higuchi and the first-order models are usually combined to describe the first very fast releasing stage and the second very slow releasing stage of the complete profile [56].

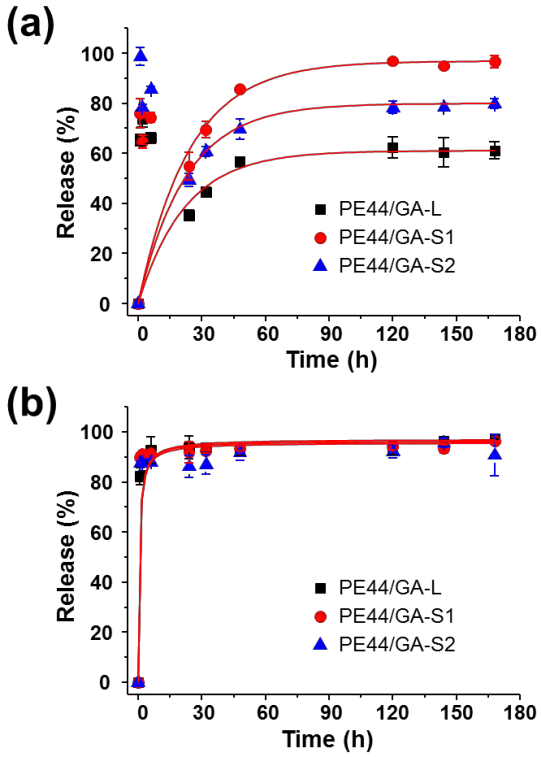

Figure 8. Accumulated release profiles of GA-S1, GA-S2 and GA-L peptides from loaded PE44 electrospun fibers in (**a**) PBS and (**b**) PBS-EtOH.

The release profiles in PBS and PBS-EtOH are frequently compared to examine the influence of the medium [57,58]. The peptide release profiles in PBS-EtOH for all PE44 loaded fibers are represented in Figure 8b. The more hydrophobic PBS-EtOH environment significantly alters the release of the three peptides, which display a very fast delivery. Specifically, the peptide retention after 6 h and 120 h was around 9% and 7%, respectively, in all cases. The differences observed between the profiles in PBS and PBS-EtOH have been attributed to the hydrophobicity of the three peptides, GA ··· solvent interactions being more favorable in the latter environment than in the former one. Accordingly, these attractive interactions are probably responsible for the diffusion of the peptides through the PE44 fibers and their subsequent delivery.

3.5. Antimicrobial Activity

The results from susceptibility tests and bacterial growth of representative Gram-negative and Gram-positive bacteria (*E. coli* and *S. aureus*, respectively) are shown in Figure S2. The presence of inhibition halos in the agar plates reflects the diffusion of the compounds with antimicrobial activity, the size of the inhibition zone being related to the level of antimicrobial activity. Accordingly, the bactericidal response against *E. coli* is slightly greater for PE44/GA-S1 and PE44/GA-S2 than for PE44/GA-L, while the activity against *S. aureus* is apparently much higher for the latter than for the formers. Obviously, the inhibition zone around gentamicin (GM), which was used as positive control, is the greatest, while the antimicrobial activity of peptide-loaded PE44 samples depends on the release rate. No inhibition halo was observed around unloaded PE44 fibers (not shown), which were used as negative control, proving that such polymeric matrix has not antibiotic activity.

Inhibition zones do not necessarily indicate that microorganisms have been killed by the antimicrobial product but just that they have been prevented from growing. In order to quantify the extent of the antimicrobial activity, the turbidity of bacteria cultures incubated in the presence of unloaded and loaded PE44 fibers was evaluated spectroscopically and was related to the bacterial growth. Figure 9 shows the bacterial growth in media containing unloaded and peptide-loaded PE44 fibers, relative to the growth in absence of any material (control). Concentrations of GA peptides in the culture media were in the 0.1 mg/mL–0.08 mg/mL range in agreement also with the values determined from the release experiments. As it can be seen, PE44/GA-S1 and, especially, PE44/GA-S2 inhibit the growth of Gram-negative bacteria, whereas unloaded PE44 and PE44/GA-L fibers are harmless to such bacteria. It is worth noting that GA-L is active against Gram-positive bacteria and against a few selected Gram-negative microbial (e.g., *Neisseria bacteria*) [36], explaining the inactivity displayed in Figure 9a. In contrast, GA-S is indistinctly effective against some Gram-positive and Gram-negative bacteria. Accordingly, the peptide-loaded PE44 fibers show antibiotic activity against Gram-positive (e.g., *S. aureus*), which decreases as follows: GA-L > GA-S2 > GA-S1 (Figure 9b). Thus, for example, after 24 h, the microbicide activity of GA-S1 and GA-S2 against *E. coli* is 9 ± 4% and 16 ± 4% inhibition of bacterial growth and 12 ± 3% and 21 ± 5% inhibition of bacterial growth against *S. aureus*, respectively. Overall, the antimicrobial activity of GA-S2 is greater than that of GA-S1, indicating that *S*,*S*-$c_3$diPhe preserves better the bioactive conformation of the parent GA-S peptide than Ac_3c. This observation is in good agreement with the CD results discussed above.

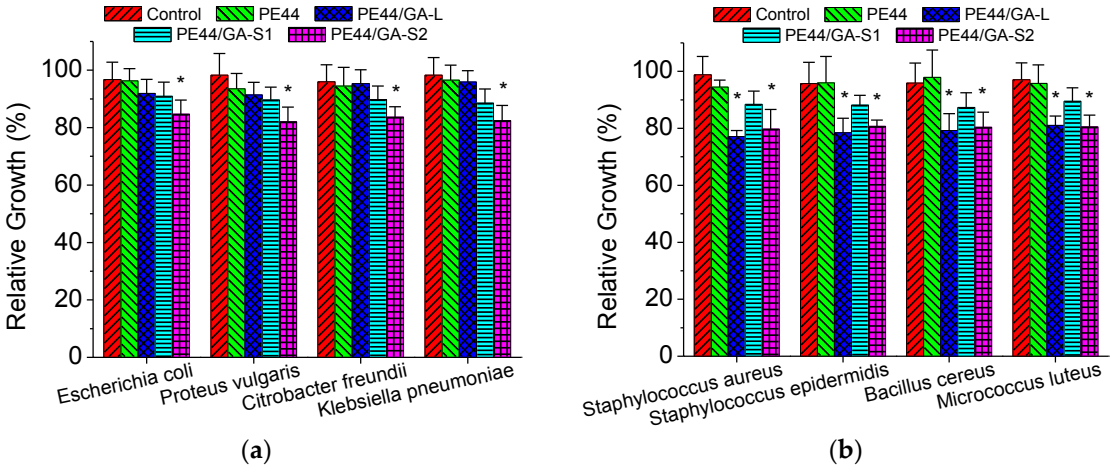

Figure 9. Bacterial growth of (**a**) Gram-negative and (**b**) Gram-positive bacteria after 24 h for unloaded and peptide-loaded PE44 fibers. Results are expressed with respect to the bacterial growth in absence of any material (control), which was considered as the maximum growth.

Although the antimicrobial behavior of PE44 fibers loaded with GA-S1 and GA-S2 is limited by the peptide release rate, the activities displayed in Figure 9 are in good agreement with those reported for the peptides in solution [36]. More specifically, biological assays of such two peptides in solution using two Gram-negative (two different *Acinetobacter baummanii* strains) and two Gram-positive (*S. aureus* and *Listeria monocytogenes*) bacteria showed that GA-S1 and GA-S2 required relative high concentrations (i.e., > 30 μM–40 μM) to show a bactericide activity. Furthermore, reported results indicated a higher activity for GA-S2 against Gram-positive bacteria. The lower activity of GA-S1 was attributed to the absence of an aromatic moiety in the Ac_3c residue (Scheme 1), which destabilized the bioactive conformation of the GA-S parent peptide [36].

3.6. Biocompatibility

The biocompatibility of PE44/GA-S1 and PE44/GA-S2 fibers was evaluated by performing in vitro cytotoxicity and cell adhesion assays, and the results were compared with those obtained for unloaded PE44 and P44/GA-L fibers. Thus, in order to do so, samples from the electrospun mats were placed in contact with a MDCK epithelial cell line inside tissue culture polystyrene (TCPS) well plates and tested using the colorimetric MTT assay to evaluate the cell viability on each well after 24 h. Viability measures were relative to TCPS without fibers, which were used as control (i.e., 100% cell viability).

As it is displayed in Figure 10a, the cytotoxicity of the three peptide-loaded systems was higher than that of unloaded PE44, the biocompatibility of the latter being similar to that of TCPS. Hence, the possible cytotoxicity of GA-S1 and GA-S2 loaded fibers should be attributed to their non-proteinogenic residues. Interestingly, the cytotoxic behavior of PE44/GA-S1 and PE44/GA-S2 was completely different, while PE44/GA-S2 behaved similarly to PE44/GA-L. Although the concentration of loaded peptide is higher GA-L than for the GA-S2 (i.e., 1.3 wt % and 0.2 wt %, respectively), this result indicates that the incorporation of *S*,*S*-c$_3$diPhe is essentially harmless to eukaryotic cells. Thus, the phenyl substituents seem to be recognized by the cells even though are tightly held in *S*,*S*-c$_3$diPhe, suggesting some similarity with the aromatic ring of L-Phe. This is probably ascribed to the proper orientation and location at different β-carbon atoms of the aromatic rings in *S*,*S*-c$_3$diPhe. In contrast, PE44/GA-S1 fibers are significantly more toxic to cells, which has been exclusively associated with the Ac$_3$c residue (i.e., two Ac$_3$c-containing antibiotics were reported to exhibit cytotoxic activity [59]).

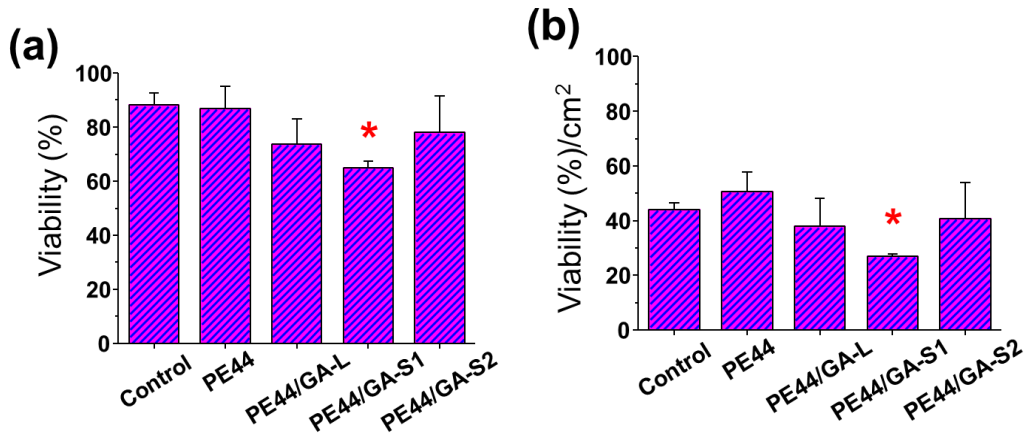

Figure 10. (**a**) viability of MDCK cells in presence of TCPS (control), unloaded PE44, PE44/GA-S1, PE44/GA-S2 and PE44/GA-L samples; (**b**) cellular adhesion onto TCPS (control) and fiber mats with unloaded or peptide-loaded fibers.

Finally, Figure 10b represents the amount of cells adhered onto the surface of the examined materials (expressed by unit of area) after 24 h. As it can be seen, in comparison to the control TCPS, cell adhesion was promoted for unloaded PE44, whereas the difference between TCPS and both PE44/GA-S2 and PE44/GA-L is not statistically significant. These observations are fully consistent with the cytotoxicity of the system (Figure 10a), which indicates that the very high biocompatibility of PE44 is slightly reduced by the loading of GA-S2 and GA-L peptides. This effect is more pronounced for PE44/GA-S1, which exhibited the lowest biocompatibility.

4. Conclusions

In this article, we describe the successful preparation and properties of electrospun polyester fibers loaded with peptide antibiotics that were designed to enhance the stability of the bioactive conformation and be resistant against proteolytic cleavage. We have proved that GA-S1 and GA-S2

cause important changes in the morphology, diameter, and properties (thermal stability and wettability) of PE44 fibers, whereas the characteristics of unloaded and GA-L loaded fibers are very similar. An important advantage of these peptide-loaded fibers as therapeutic platforms is that the polymeric matrix regulates the release of the antibiotic in hydrophilic environments similar to physiological media. The antimicrobial activity of PE44/GA-S1 and PE44/GA-S2 is comparable (Gram-negative) or higher (Gram-positive) than that of PE44/GA-L. Moreover, the antibiotic potency of both GA-S1 and GA-S2 is higher when loaded into polyester fibers than in solution, suggesting that the PE44 matrix enhances the stability of their bioactive conformation. Overall, these findings reflect that formulations such as biodegradable polymeric fibers loaded with engineered peptides are promising platforms for biomedical applications.

Supplementary Materials: FTIR spectra of electrospun unloaded and GA-loaded PE44 fibers and inhibition halos of representative Gram-negative and Gram-positive bacteria.

Acknowledgments: The authors thank support from Ministerio de Economía y Competitividad (MINECO) and Fondo Europeo de Desarrollo Regional (FEDER) (MAT2015-69367-R, MAT2015-69547-R and CTQ2013-40855-R) and Gobierno de Aragón—FEDER (research group E40). Support for the research of C.A. was received through the prize "ICREA Academia" for excellence in research funded by the Generalitat de Catalunya.

Author Contributions: S.M. and M.M.P.-M. performed experiments. C.C. was involved in the synthesis of gramicidin analogues and contributed in discussion. L.J.d.V., J.P. and C.A. supervised project direction and contributed in discussion.

Conflicts of Interest: The authors declare no conflict of interest.

References

1. Wan, W.K.; Yang, L.; Padavan, D.T. Use of degradable and nondegradable nanomaterials for controlled release. *Nanomedicine* **2007**, *2*, 483–509. [CrossRef] [PubMed]
2. Timko, B.P.; Kohane, S. Materials to clinical devices: Technologies for remotely triggered drug delivery. *Clin. Ther.* **2012**, *34*, S25–S35. [CrossRef] [PubMed]
3. LaVan, D.A.; McGuire, T.; Langer, R. Small-scale systems for in vivo drug delivery. *Nat. Biotechnol.* **2003**, *21*, 1184–1191. [CrossRef] [PubMed]
4. Mura, S.; Nicolas, J.; Couvreur, P. Stimuli-responsive nanocarriers for drug delivery. *Nat. Mater.* **2013**, *12*, 991–1003. [CrossRef] [PubMed]
5. Timko, B.P.; Dvir, T.; Kohane, D.S. Remotely triggerable drug delivery systems. *Adv. Mater.* **2010**, *22*, 4925–4943. [CrossRef] [PubMed]
6. Balmert, S.C.; Little, S.R. Biomimetic delivery with micro and nanoparticles. *Adv. Mater.* **2012**, *24*, 3757–3778. [CrossRef] [PubMed]
7. Gao, J.; Li, W.; Guo, Y.J.; Feng, S.S. Nanomedicine strategies for sustained, controlled and targeted treatment of cancer stem cells. *Nanomedicine* **2016**, *11*, 3261–3282. [CrossRef] [PubMed]
8. Orawan, S. Biomedical application of electrospun polycaprolactone fiber mats. *Polym. Adv. Technol.* **2016**, *27*, 1264–1273.
9. Natarjan, J.; Dasgupta, Q.; Shetty, S.N.; Sarkar, K.; Madras, G.; Chatterjee, K. Poly(ester amide)s from Soybean Oil for Modulated Release and Bone Regeneration. *ACS Appl. Mater. Interfaces* **2016**, *8*, 25170–25184. [CrossRef] [PubMed]
10. Pushpamalar, J.; Veeramachineni, A.K.; Owh, C.; Loh, X.J. Biodegradable polysaccharides for controlled drug delivery. *ChemPlusChem* **2016**, *81*, 504–514. [CrossRef]
11. Cardoso, M.J.; Caridade, S.G.; Costa, R.R.; Mano, J.F. Enzymatic degradation of polysaccharide-based layer-by-layer structures. *Biomacromolecules* **2016**, *17*, 1347–1357. [CrossRef] [PubMed]
12. Winnacker, M.; Rieger, B. Poly(ester amide)s: Recent insights into synthesis, stability and biomedical applications. *Polym. Chem.* **2016**, *7*, 7039–7046. [CrossRef]
13. Manavitehrani, I.; Fathi, A.; Badr, H.; Daly, S.; Shirazi, A.N.; Deghani, F. Biomedical applications of biodegradable polyesters. *Polymers* **2016**, *8*, 20. [CrossRef]
14. Stebbins, N.D.; Faig, J.J.; Yu, W.; Guliyev, R.; Uhrich, K.E. Polyactives: Controlled and sustained bioactive release via hydrolytic degradation. *Biomater. Sci.* **2015**, *3*, 1171–1187. [CrossRef] [PubMed]

15. Du, C.; Zhao, J.; Fei, J.; Cui, Y.; Li, J. Assembled microcapsules by doxorubicin and polysaccharide as high effective anticancer drug carriers. *Adv. Healthc. Mater.* **2013**, *2*, 1246–1251. [CrossRef] [PubMed]
16. Gao, L.; Cui, Y.; He, Q.; Yang, Y.; Fei, J.; Li, J. Selective recognition of co-assembled thrombin aptamer and docetaxel on mesoporous silica nanoparticles against tumor cell proliferation. *Chem. Eur. J.* **2011**, *17*, 13170–13174. [CrossRef] [PubMed]
17. Yan, H.; Hou, Y.-F.; Niu, P.-F.; Zhang, K.; Shoji, T.; Tsuboi, Y.; Yao, F.-Y.; Zhao, L.-M.; Chang, J.-B. Biodegradable PLGA nanoparticles loaded with hydrophobic drugs: Confocal Raman microspectroscopic characterization. *J. Mater. Chem. B* **2015**, *3*, 3677–3680. [CrossRef]
18. Ashwanikumar, N.; Kumar, N.A.; Nair, S.A.; Kumar, G.S.V. 5-Fluorouracil-lipid conjugate: Potential candidate for drug delivery through encapsulation in hydrophobic polyester-based nanoparticles. *Acta Biomater.* **2014**, *10*, 4685–4694. [CrossRef] [PubMed]
19. Maione, S.; del Valle, L.J.; Pérez-Madrigal, M.M.; Cativiela, CC.; Puiggalí, J.; Alemán, C. Electrospray loading and release of hydrophobic gramicidin in polyester microparticles. *RSC Adv.* **2016**, *6*, 73045–73055. [CrossRef]
20. Pérez-Madrigal, M.M.; Llorens, E.; del Valle, L.J.; Puiggalí, J.; Armelin, E.; Alemán, C. Semiconducting, biodegradable and bioactive fibers for drug delivery. *Express Polym. Lett.* **2016**, *10*, 628–646. [CrossRef]
21. Planellas, M.; Pérez-Madrigal, M.M.; del Valle, L.J.; Kobauri, S.; Katsarava, R.; Alemán, C.; Puiggalí, J. Microfibres of conducting polythiophene and biodegradable poly(ester urea) for scaffolds. *Polym. Chem.* **2015**, *6*, 925–937. [CrossRef]
22. Liou, J.W.; Hung, Y.J.; Yang, C.H.; Chen, Y.C. The antimicrobial activity of Gramicidin A is associated with hydroxyl radical formation. *PLoS ONE* **2015**, *10*, e0117065. [CrossRef] [PubMed]
23. Yala, J.F.; Thebault, P.; Hequet, A.; Humblot, V.; Pradier, C.M.; Berjeaud, J.M. Elaboration of antibiofilm materials by chemical grafting of an antimicrobial peptide. *Appl. Microbiol. Biotechnol.* **2011**, *89*, 623–634. [CrossRef] [PubMed]
24. Wang, F.; Qin, L.H.; Pace, C.J.; Wong, P.; Malonis, R.; Gao, J.M. Solubilized Gramicidin A as potential systemic antibiotics. *ChemBioChem* **2012**, *13*, 51–55. [CrossRef] [PubMed]
25. David, J.M.; Owens, T.A.; Barwe, S.P.; Rajasekaran, A.K. Gramicidin A induces metabolic dysfunction and energy depletion leading to cell death in renal cell carcinoma cells. *Mol. Cancer Ther.* **2013**, *12*, 2296–2307. [CrossRef] [PubMed]
26. David, J.M.; Owens, T.A.; Inge, L.J.; Bremmer, R.M.; Rajasekaran, A.K. Gramicidin A blocks tumor growth and angiogenesis through inhibition of hypoxia-inducible factor in renal cell carcinoma. *Mol. Cancer Ther.* **2014**, *13*, 788–799. [CrossRef] [PubMed]
27. Wijesinghe, D.; Arachchige, M.C.; Lu, A.; Reshetnyak, Y.K.; Andreev, O.A. pH dependent transfer of nano-pores into membrane of cancer cells to induce apoptosis. *Sci. Rep.* **2013**, *3*, 3650. [CrossRef] [PubMed]
28. Rao, D.K.; Liu, H.Y.; Ambudkar, S.V.; Mayer, M. A combination of curcumin with either gramicidin or ouabain selectively kills cells that express the multidrug resistance-linked ABCG2 transporter. *J. Biol. Chem.* **2014**, *289*, 31397–31410. [CrossRef] [PubMed]
29. Abdelhamid, H.N.; Khan, M.S.; Wu, H.-F. Graphene oxide as a nanocarrier for gramicidin (GOGD) for high antibacterial performance. *RSC Adv.* **2014**, *4*, 50035–50046. [CrossRef]
30. Dittrich, C.; Meier, W. Solid peptide nanoparticles—Structural characterization and quantification of cargo encapsulation. *Macromol. Biosci.* **2010**, *10*, 1406–1415. [CrossRef] [PubMed]
31. Schuster, T.B.; de Bruyn Outboter, D.; Bordignon, E.; Jeschke, G.; Meier, W. Reversible peptide particle formation using a mini amino acid sequence. *Soft Matter* **2010**, *6*, 5596–5604. [CrossRef]
32. Wang, K.; Ruan, J.; Song, H.; Zhang, J.; Wo, Y.; Guo, S.; Cui, D. Biocompatibility of graphene oxide. *Nanoscale Res. Lett.* **2011**, *6*, 8. [CrossRef] [PubMed]
33. Biron, E.; Chatterjee, J.; Ovadia, O.; Langenegger, D.; Brueggen, J.; Hoyer, D.; Schmid, H.A.; Jelinek, R.; Gilon, C.; Hoffman, A.; et al. Improving oral bioavailability of peptides by multiple *N*-methylation: somatostatin analogues. *Angew. Chem. Int. Ed.* **2008**, *47*, 2595–2599. [CrossRef] [PubMed]
34. Horne, W.S.; Gellman, S.H. Foldamers with heterogeneous backbones. *Acc. Chem. Res.* **2008**, *41*, 1399–1408. [CrossRef] [PubMed]
35. Sadowsky, J.D.; Murray, J.K.; Tomita, Y.; Gellman, S.H. Exploration of backbone space in foldamers containing α- and β-amino acid residues: Developing Protease-resistant oligomers that bind tightly to the BH3-recognition cleft of Bcl-xL. *ChemBioChem* **2007**, *8*, 903–916. [CrossRef] [PubMed]

36. Solanas, C.; de la Torre, B.G.; Fernández-Reyes, M.; Santiverri, C.; Jiménez, M.A.; Rivas, L.; Jiménez, A.I.; Andreu, D.; Cativiela, C. Sequence inversion and phenylalanine surrogates at the β-turn enhance the antibiotic activity of Gramicidin S. *J. Med. Chem.* **2010**, *53*, 4119–4129. [CrossRef] [PubMed]
37. Gause, G.F. Gramicidin S and its use in the treatment of infected wounds. *Nature* **1944**, *154*, 703. [CrossRef]
38. Kondejewski, L.H.; Farmer, S.W.; Wishart, D.S.; Hancock, R.E.; Hodges, R.S. Gramicidin S is active against both Gram-positive and Gram-negative bacteria. *Int. J. Pept. Protein. Res.* **1996**, *47*, 460–466. [CrossRef] [PubMed]
39. Prenner, E.J.; Lewis, R.N.; McElhaney, R.N. The interaction of the antimicrobial peptide gramicidin S with lipid bilayer model and biological membranes. *Biochim. Biophys. Acta* **1999**, *1462*, 201–221. [CrossRef]
40. Alemán, C. Conformational properties of α-amino acids disubstituted at the α-carbon. *J. Phys. Chem. B* **1997**, *101*, 5046–5050. [CrossRef]
41. Alemán, C.; Jiménez, A.I.; Cativiela, C.; Pérez, J.J.; Casanovas, J. Influence of the phenyl side chain on the conformation of cyclopropane analogues of phenylalanine. *J. Phys. Chem. B* **2002**, *106*, 11849–11858. [CrossRef]
42. Casanovas, J.; Jiménez, A.I.; Cativiela, C.; Pérez, J.J.; Alemán, C. *N*-Acetyl-*N*′-methylamide derivative of (2*S*,3*S*)-1-amino-2,3-diphenylcyclopropane carboxylic acid: Theoretical analysis of the conformational impact produced by the incorpororation of the second phenyl group to the cyclopropane analogue of phenylalanine. *J. Org. Chem.* **2003**, *68*, 7088–7091. [CrossRef] [PubMed]
43. Frenot, A.; Chronakis, I.S. Polymer nanofibers assembled by electrospinning. *Curr. Opin. Colloid Interface Sci.* **2003**, *8*, 64–75. [CrossRef]
44. Li, D.; Xia, Y. Electrospinning of nanofibers: Reinventing the wheel? *Adv. Mater.* **2004**, *16*, 1151–1170. [CrossRef]
45. Jayaraman, K.; Kotaki, M.; Zhang, Y.; Mo, X.; Ramakrishna, S. Recent advances in polymer nanofibers. *J. Nanosci. Nanotechnol.* **2004**, *4*, 52–65. [PubMed]
46. Whitmore, L.; Wallace, B.A. Protein secondary structure analyses from circular dichroism spectroscopy: Methods and reference databases. *Biopolymers* **2008**, *89*, 392–400. [CrossRef] [PubMed]
47. Whitmore, L.; Wallace, B.A. DICHROWEB, an online server for protein secondary structure analyses from circular dichroism spectroscopic data. *Nucleic Acids Res.* **2004**, *32*, 668–673. [CrossRef] [PubMed]
48. On-line analysis for protein Circular Dichroism spectra. Available online: http://dichroweb.cryst.bbk.ac.uk (accessed on 11 May 2017).
49. Chen, Y.; Wallace, B.A. Solvent effects on the conformation and far UV CD spectra of gramicidin. *Biopolymers* **1997**, *42*, 771–781. [CrossRef]
50. Llorens, E.; Ibañez, H.; del Valle, L.J.; Puiggalí, J. Biocompatibility and drug release behavior of scaffolds prepared by coaxial electrospinning of poly(butylene succinate) and polyethylene glycol. *Mater. Sci. Eng. C* **2015**, *49*, 472–484. [CrossRef] [PubMed]
51. Wang, H.Y.; Ji, J.H.; Zhang, W.; Zhang, Y.H.; Jiang, J.; Wu, Z.W.; Pu, S.H.; Chu, P.K. Biocompatibility and bioactivity of plasma-treated biodegradable poly(butylene succinate). *Acta Biomater.* **2009**, *5*, 279–287. [CrossRef] [PubMed]
52. Moulder, J.F.; Stickle, W.F.; Sobol, P.E.; Bomben, K.D. *Handbook of X-Ray Photoelectron Spectroscopy*; Perkin-Elmer Corp: Eden Prairie, MN, USA, 1992.
53. Yang, Z.; Yuan, S.; Liang, B.; Liu, Y.; Choong, C.; Pehkonen, S.O. Chitosan microsphere scaffold tethered with RGD-conjugated poly(methacrylic acid) brushes as effective carriers for the endothelial cells. *Macromol. Biosci.* **2014**, *14*, 1299–1311. [CrossRef] [PubMed]
54. Smith, G.C. Evaluation of a simple correction for the hydrocarbon contamination layer in quantitative surface analysis by XPS. *J. Electron. Spectrosc. Relat. Phenom.* **2005**, *148*, 21–28. [CrossRef]
55. Marmur, A. Soft contact: Measurement and interpretation of contact angles. *Soft Matter* **2006**, *2*, 12–17. [CrossRef]
56. Jeong, E.H.; Im, S.S.; Youk, J.H. Electrospinning and structural characterization of ultrafine poly (butylene succinate) fibers. *Polymer* **2005**, *46*, 9538–9543. [CrossRef]
57. Del Valle, L.J.; Camps, R.; Díaz, A.; Franco, L.; Rodríguez-Galán, A.; Puiggalí, J. Electrospinning of polylactide and polycaprolactone mixtures for preparation of materials with tunable drug release properties. *J. Polym. Res.* **2011**, *18*, 1903–1917. [CrossRef]

58. Murase, S.; Aymat, M.; Calvet, A.; del Valle, L.J.; Puiggalí, J. Electrosprayed poly (butylene succinate) microspheres loaded with indole derivatives: A system with anticancer activity. *Eur. Polym. J.* **2015**, *71*, 196–209. [CrossRef]
59. Nishio, M.; Kohno, J.; Sakurai, M.; Suzuki, S.; Okada, N.; Kawano, K.; Komatsubara, S. TMC-135A and B, new triene-ansamycins, produced by Streptomyces sp. *J. Antibiot.* **2000**, *53*, 724–727. [CrossRef] [PubMed]